Available online at www.sciencedirect.com
SCIENCE DIRECT®
Journal of Magnetic Resonance 167 (2004) 75–86
JMR Journal of Magnetic Resonance
www.elsevier.com/locate/jmr

Chemical shift anisotropy amplification

Limin Shao,[a] Charles Crockford,[b] Helen Geen,[b] Giuseppe Grasso,[a] and Jeremy J. Titman[a,*]

[a] School of Chemistry, University of Nottingham, University Park, Nottingham NG7 2RD, UK
[b] School of Physics and Astronomy, University of Nottingham, University Park, Nottingham NG7 2RD, UK

Received 13 August 2003; revised 21 November 2003

Abstract

A new NMR experiment which allows a measurement of the chemical shift anisotropy (CSA) tensor under magic angle spinning (MAS) is described. This correlates a fast MAS spectrum in the ω_2 dimension with a sideband pattern in ω_1 in which the intensities mimic those for a sample spinning at a fraction of the rate ω_r/N, and these sidebands result from an amplification by a factor N of the modulation caused by the CSA. Standard methods can be used to extract the principal tensor components from the ω_1 sideband patterns, and the nature of the experiment is such that the use of a large number of t_1 increments can avoided without compromising the resolution of different chemical sites. The new experiment is useful for accurately measuring narrow shift anisotropies.

Keywords: Chemical shift anisotropy; Magic angle spinning; Spinning sidebands

1. Introduction

The singularities observed in the broad NMR lines of a powdered sample correspond directly to the principal values of the chemical shift anisotropy (CSA) tensor [1], determination of which provides detailed information about the molecular structures of solids. In order to avoid spectral overlap and perturbations from dipolar couplings, measurements of the CSA are made by analyzing the intensities of the rotational sidebands [2,3] which appear in the magic angle spinning (MAS) spectrum. A relatively low spinning rate ω_r is normally required to provide sufficient sidebands for analysis, resulting in problems with overlap of different sideband manifolds in molecules with many chemical sites. Hence, many two-dimensional MAS NMR experiments have been developed to separate the isotropic and anisotropic parts of the chemical shift interaction and to further improve resolution [4–15].

Of these, experiments based on the PASS technique [16] are some of the simplest to implement and most efficient in terms of acquisition time. In PASS sequences of π-pulses synchronized with the MAS result in a phase shift of magnitude $M\Theta$ for the sideband at a frequency $M\omega_r$ from the isotropic line. The angle Θ is known as the "pitch" of the sequence. Two-dimensional variants of PASS [17,18] employ constant duration sequences with arbitrary pitch which allow Θ to be varied over a full period in the evolution dimension. A Fourier transform with respect to pitch results in the separation of different sideband manifolds over the ω_1 co-ordinate of the two-dimensional spectrum. The isotropic shifts are restricted to the ω_2 dimension and the anisotropic part in sampled as a sideband pattern in ω_1. Since the sidebands are regularly spaced and there is no decay of the magnetization in the evolution period, a minimal number of t_1 increments suffices and long acquisition times are avoided.

Recently, we have briefly described a new two-dimensional MAS experiment [19] which is closely related to 2D-PASS. The new experiment correlates the standard MAS spectrum in the ω_2 dimension with a sideband pattern in ω_1 in which the intensities are identical to those expected for a sample spinning at some fraction $1/N$ of the actual rate ω_r. The sideband pattern in the ω_1 dimension results from an amplification by a factor N of the modulation caused by the CSA, a process referred to here as "CSA amplification." In common with 2D-PASS the isotropic shift appears only in the ω_2

* Corresponding author. Fax: +44-115-95-13562.
E-mail address: jeremy.titman@nott.ac.uk (J.J. Titman).

1090-7807/$ - see front matter © 2003 Elsevier Inc. All rights reserved.
doi:10.1016/j.jmr.2003.11.005

dimension, and long acquisition times can be avoided without loss of resolution of different chemical sites. In contrast to 2D-PASS, the new experiment is appropriate for measuring narrow shift anisotropies, overcoming the need for extremely slow MAS rates which lead to rotor instability.

As an illustration Fig. 1(A) shows the centerband portion of the standard carbon-13 MAS spectrum of methyl-α-D-glucopyranoside recorded at a rate of 4 kHz and a Larmor frequency of 75.47 MHz At this MAS rate there are no spinning sidebands in the spectrum, since the chemical shift anisotropies are relatively small. Fig. 1(B) shows a two-dimensional spectrum of methyl-α-glucopyranoside recorded using the new experiment with a MAS rate of 4 kHz and an amplification factor of 8, resulting in an apparent rate of 500 Hz in the ω_1 dimension. Further experimental details are given in the figure caption. There are a substantial number of spinning sidebands for each carbon-13 site in ω_1. The pulse sequence used to record the two-dimensional MAS spectrum in Fig. 1(B) is shown in Fig. 2. Enhanced carbon-13 transverse magnetization generated by cross polarization evolves under a sequence consisting of a small number q of carefully timed π-pulses. Subsequently one component of the magnetization is stored on the z-axis for a time t_1, before a further period of evolution under an identical q-pulse sequence prior to detection during t_2. The t_1 time is incremented by some convenient fraction, usually 1/16 or 1/32, of the rotor period. Further details are given below.

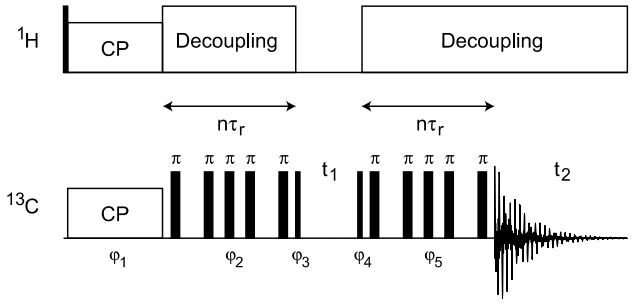

Fig. 2. The pulse sequence used to record CSA amplification spectra. Narrow and broad black rectangles represent π/2- and π-pulses, respectively. Further experimental details as well as timings for the π-pulses are given in the text.

In our previous publication [19] a brief description of CSA amplification was given, along with timings suitable for sequences with five π-pulses symmetrically disposed within an integral number of rotor periods. More recently, we have shown how the combination of CSA amplification and rotor-synchronization can be used to measure orientation distributions in macroscopically ordered samples [20]. In the current paper, we give a full treatment of the necessary theory and derive new analytical solutions for the timings in sequences of four and seven π-pulses. The latter have enhanced amplification factors compared to those with five π-pulses, while the former minimize the number of pulses required in the experiment. We show that accurate values of the principal components of chemical shift tensors can be measured using CSA amplification and assess the

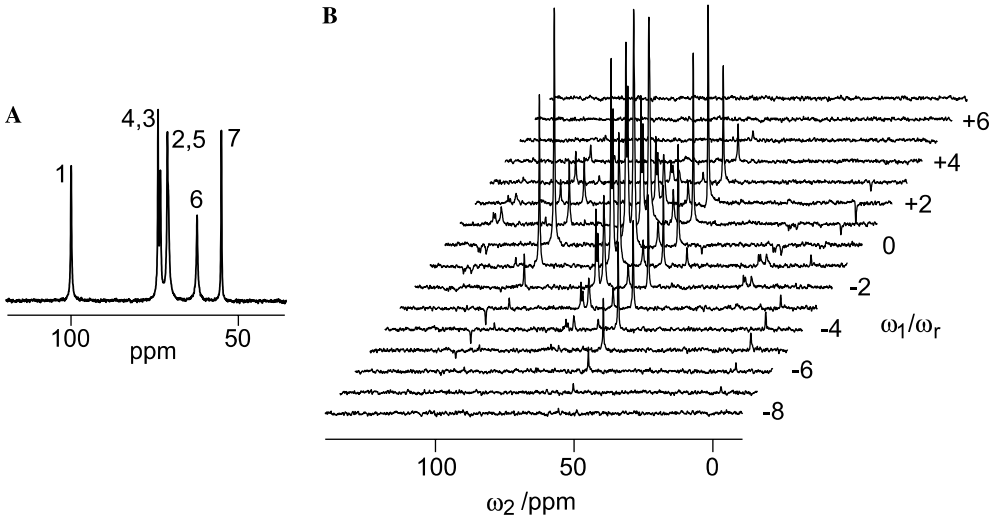

Fig. 1. (A) Part of the carbon-13 MAS spectrum of methyl-α-D-glucopyranoside recorded at a rate of 4 kHz using a 7.5 mm MAS probe and a standard cross polarization pulse sequence with a contact time of 4.1 ms. The MAS rate was stabilized to ±1 Hz. Proton decoupling with a field strength of 55 kHz was applied throughout the acquisition period which lasted 68 ms. The full spectral width was 30 kHz and 32 scans were acquired. (B) Part of a carbon-13 CSA amplification spectrum of methyl-α-glucopyranoside recorded with a MAS rate of 4 kHz and an amplification factor of 8. The spectrum was recorded and processed as described in the Experimental section. Note the substantial number of spinning sidebands for each carbon-13 site in the ω_1 dimension which corresponds to a reduced MAS rate of 500 Hz. There were 32 t_1 values in total with an increment of 7.81 μs, corresponding to 1/32 of the MAS period. Other experimental parameters were as for (A) except that 48 scans were acquired per increment, and the carbon-13 π-pulse length was 7.7 μs.

reliability of these measurements in the presence of experimental imperfections and resonance offset.

2. Theory of CSA amplification

2.1. MAS sideband intensities

The orientation of the CSA principal axis frame of a particular spin site relative to the MAS rotor is given by the Euler angles (α, β, γ). Following Antzutkin et al. [21] we consider a "carousel" of sites which have a single value of α and β, but a uniform and continuous distribution of γ angles. The NMR precession frequency of sites within a carousel $\omega_c(t;\gamma)$ can be written as a Fourier series

$$\omega_c(t;\gamma) = \sum_{m=-2}^{2} \omega_c^{(m)}(\gamma) \exp(\mathrm{i}m\omega_r t). \tag{1}$$

The coefficients $\omega_c^{(m)}$ are given by

$$\omega_c^{(m)}(\gamma) = \sum_{n=-2}^{2} D^2_{n-m}(\alpha,\beta,\gamma) d^2_{-m0}(\beta_0) A_{2n} + \delta_{m0}\omega_{iso}, \tag{2}$$

where the A_{2n} are the components of the chemical shift tensor, β_0 is the magic angle and the isotropic shift ω_{iso} depends on the offset from the carrier frequency ω_{RF}

$$\omega_{iso} = \omega_0(1-\sigma_{iso}) - \omega_{RF}. \tag{3}$$

The Wigner rotations $D(\alpha,\beta,\gamma)$ and $d(\beta)$ are defined here according to the convention of Spiess in which α is the angle of rotation of the original tensor about its own z-axis. Neglecting relaxation the MAS FID for sites in the carousel can be written as [21]

$$S_c(t;\gamma) = \exp\left\{\mathrm{i}\left[\omega_c^{(0)}t + \xi_c(t;\gamma) - \xi_c(0;\gamma) + \phi_c(0;\gamma)\right]\right\}, \tag{4}$$

where ξ_c is defined by

$$\xi_c(t;\gamma) = \sum_{m\neq 0} \frac{\omega_c^{(m)}(\gamma)\exp(\mathrm{i}m\omega_r t)}{\mathrm{i}m\omega_r}. \tag{5}$$

The difference $\xi_c(t;\gamma) - \xi_c(0;\gamma)$ is the phase angle accumulated by the transverse magnetization during the acquisition time, while $\phi_c(0;\gamma)$ represents its initial phase which is independent of orientation under normal circumstances.

It has recently been shown [21] that many features of MAS, such as the uniform phase of the sidebands or their suppression in the TOSS experiment, can be explained using symmetry arguments. These arise from the fact that orientations within a carousel experience the same spin precession frequencies at different times during a MAS period. The coefficients $\omega_c^{(m)}(\gamma)$ have the symmetry

$$\omega_c^{(m)}(\gamma) = \omega_c^{(m)}(0)\exp(\mathrm{i}m\gamma), \tag{6}$$

which implies a time/orientation equivalence for $\xi_c(t;\gamma)$ of the form

$$\xi_c(t;\gamma) = \xi_c(t+\gamma/\omega_r;0) = \xi_c(0;\gamma+\omega_r t). \tag{7}$$

The intensities of the spinning sidebands can be extracted from Eq. (4) using a Fourier series expansion

$$\exp\{\mathrm{i}\xi_c(0;\varphi)\} = \sum_{j=-\infty}^{\infty} F_j \exp(\mathrm{i}j\varphi), \tag{8}$$

where the coefficients F_j are given by

$$F_j = \frac{1}{2\pi}\int_0^{2\pi} \exp\{\mathrm{i}\xi_c(0;\varphi)\}\exp(-\mathrm{i}j\varphi)\,\mathrm{d}\varphi. \tag{9}$$

Assuming zero initial phase, Eq. (4) becomes

$$S_c(t;\gamma) = \sum_{j',j=-\infty}^{\infty} F^*_{j'}F_j \exp\{\mathrm{i}\gamma(j-j')\}\exp(\mathrm{i}j\omega_r t) \times \exp\left(\mathrm{i}\omega_c^{(0)}t\right) \tag{10}$$

and integrating over γ gives the intensity I_j of the sideband at $\omega_c^{(0)} + j\omega_r$ for the carousel as

$$I_j = \sum_{j'=-\infty}^{\infty} F^*_{j'}F_j \frac{1}{2\pi}\int_0^{2\pi} \exp\{\mathrm{i}\gamma(j-j')\}\,\mathrm{d}\gamma = F^*_j F_j. \tag{11}$$

So long as the distribution of γ values is uniform and continuous the sideband intensities are real. In order to obtain the correct sideband intensities for a powder sample, further integration over the Euler angles α and β is required.

2.2. A two-dimensional experiment which correlates fast and slow spinning sideband patterns

CSA amplification by a factor N is achieved in the ω_1 dimension of a two-dimensional experiment by ensuring that phase accumulation under the anisotropic chemical shift occurs N times more rapidly in t_1 than in t_2. It will be shown below that the required two-dimensional FID is

$$S_c(t_1,t_2;\gamma) = \exp\{\mathrm{i}[-N\xi_c(0;\gamma+\omega_r t_1) + N\xi_c(0;\gamma)]\}\exp\left\{\mathrm{i}\left[\omega_c^{(0)}t_2 + \xi_c(0;\gamma+\omega_r t_2) - \xi_c(0;\gamma)\right]\right\}, \tag{12}$$

where relaxation has been neglected. Note that phase accumulation under the isotropic chemical shift is restricted to t_2 and that N is not necessarily an integer. In this case sideband intensities can be extracted using a modified Fourier series expansion

$$\exp(\mathrm{i}N\xi_c(0;\varphi)) = \sum_{j=-\infty}^{\infty} \mathrm{F}'_j \exp(\mathrm{i}j\varphi) \tag{13}$$

with coefficients

$$F'_j = \frac{1}{2\pi}\int_0^{2\pi} \exp\{\mathrm{i}N\xi_c(0;\varphi)\}\exp(-\mathrm{i}j\varphi)\,\mathrm{d}\varphi = \frac{1}{2\pi}\int_0^{2\pi} \exp\left\{\sum_{m\neq 0}\frac{\omega_c^{(m)}(0)\exp(\mathrm{i}m\varphi)}{m(\omega_r/N)}\right\}\exp(-\mathrm{i}j\varphi)\,\mathrm{d}\varphi, \tag{14}$$

which are identical to the F_j except for the replacement of ω_r by ω_r/N. Following the treatment above, the carousel signal becomes

$$S_c(t_1,t_2;\gamma)=\sum_{j',j,k',k=-\infty}^{\infty}F'_{j'}F'^{*}_{j}F^{*}_{k'}F_k\exp\{i\gamma(j'+k-j-k')\}\times\exp(ij\omega_r t_1)\exp\{i(\omega_c^{(0)}+k\omega_r)t_2\} \quad (15)$$

and the intensity of the sideband at co-ordinates ($j\omega_r$, $k\omega_r$) in the two-dimensional spectrum is

$$I_{j,k}=\sum_{j'=-\infty}^{\infty}F'_{j'}F'^{*}_{j}F^{*}_{j'-j+k}F_k \quad (16)$$

because components which do not satisfy $j'-j+k-k'=0$ vanish in the integral over γ. Projecting onto ω_1 gives the intensity of the sideband at $j\omega_r$ as

$$I_j=\sum_{k=-\infty}^{\infty}I_{j,k}=\sum_{j'=-\infty}^{\infty}F'_{j'}F'^{*}_{j}\sum_{k=-\infty}^{\infty}F^{*}_{j'-j+k}F_k. \quad (17)$$

Because of the normalization of $\exp(i\xi_c(\varphi))$, the coefficients F_k satisfy

$$\sum_{k=-\infty}^{\infty}F_{n+k}F^{*}_{k}=0,\quad n\neq 0,\qquad \sum_{k=-\infty}^{\infty}F_{n+k}F^{*}_{k}=1,\quad n=0. \quad (18)$$

Hence, the only non-zero component in Eq. (17) occurs for $j=j'$ when the summation over k is unity and

$$I_j=F'_jF'^{*}_j. \quad (19)$$

Because the definition of F'_j in Eq. (14) is identical to that of F_j in Eq. (9) except for the replacement of ω_r by ω_r/N, the sideband intensities in the projection onto the ω_1 dimension are identical to those which would be observed with the CSA amplified by a factor N. Note, however, that the sidebands appear at integer multiples of the actual MAS rate ω_r in ω_1.

2.3. CSA amplification sequences

The method of CSA amplification described here involves the use of sequences of π-pulses to manipulate the initial phase term in Eq. (4). It is shown here that for amplification by a factor N the phase accumulated by the end of the sequence $\phi_c(0;\gamma)$ must be equal to $N\xi_c(0;\gamma)$ for all sites in the carousel. In the following discussion, the time origin is assumed to be at the end of the sequence which has total duration T with pulses applied at timings $t^{(p)}-T$. The experiment shown in Fig. 2 uses two identical sequences which are separated by an time t_1 during which a component of the magnetization is stored on the z-axis. The magnitude of the stored component depends only on the phase accumulated during the first of the two sequences and the phase φ_3 of the first carbon-13 $\pi/2$ pulse. From Eq. (4) the two parts of the two-dimensional signal recorded with φ_3 set to $\pi/2$ and π, respectively are

$$\begin{aligned}S_c^{Re}(t_1,t_2;\gamma)&=\cos\{N\xi_c(0;\gamma)\}\\&\times\exp\{i[\omega_c^{(0)}t_2+\xi_c(0;\gamma+\omega_r t_1+\omega_r t_2)\\&-\xi_c(0;\gamma+\omega_r t_1)+N\xi_c(0;\gamma+\omega_r t_1)]\},\\S_c^{Im}(t_1,t_2;\gamma)&=\sin\{N\xi_c(0;\gamma)\}\\&\times\exp\{i[\omega_c^{(0)}t_2+\xi_c(0;\gamma+\omega_r t_1+\omega_r t_2)\\&-\xi_c(0;\gamma+\omega_r t_1)+N\xi_c(0;\gamma+\omega_r t_1)]\}.\end{aligned} \quad (20)$$

These two parts are combined in the receiver to give

$$\begin{aligned}S_c(t_1,t_2;\gamma)&=S_c^{Re}(t_1,t_2;\gamma)-iS_c^{Im}(t_1,t_2;\gamma)\\&=\exp\{-iN\xi_c(0;\gamma)\}\exp\{i[\omega_c^{(0)}t_2\\&+\xi_c(0;\gamma+\omega_r t_1+\omega_r t_2)\\&-\xi_c(0;\gamma+\omega_r t_1)+N\xi_c(0;\gamma+\omega_r t_1)]\}\end{aligned} \quad (21)$$

and a trivial change of variable $\gamma'=\gamma+\omega_r t_1$ results in

$$\begin{aligned}S_c(t_1,t_2;\gamma)&=\exp\{-iN\xi_c(0;\gamma'-\omega_r t_1)\}\\&\times\exp\{i[\omega_c^{(0)}t_2+\xi_c(0;\gamma'+\omega_r t_2)\\&-\xi_c(0;\gamma')+N\xi_c(0;\gamma')]\},\end{aligned} \quad (22)$$

which is identical to Eq. (12) apart from the reversal of the t_1 axis.

It follows from the above that CSA amplification can be achieved if the timings of the q π-pulses in both sequences are chosen so that $\phi_c(0;\gamma)=N\xi_c(0;\gamma)$. The phase accumulated during a sequence containing q π-pulses is [21]

$$\phi_c(0;\gamma)=\omega_c^{(0)}\tau+\xi_c(0;\gamma)-(-1)^q\left\{2\sum_{p=1}^{q}(-1)^p\xi_c(t^{(p)}-T;\gamma)+\xi_c(-T;\gamma)\right\}, \quad (23)$$

where an infinitely strong RF field has been assumed and

$$\tau=T-2\sum_{p=1}^{q}(-1)^{p-q}t^{(p)}. \quad (24)$$

When $\tau=0$ the end of the sequence coincides with a spin echo and phase shifts for different sites are avoided. In this situation CSA amplification by a factor N results from pulse timings $t^{(p)}$ which satisfy

$$(N-1)\xi_c(0;\gamma)+(-1)^q\left\{2\sum_{p=1}^{q}(-1)^p\xi_c(t^{(p)}-T;\gamma)+\xi_c(-T;\gamma)\right\}=0. \quad (25)$$

Using the definition of ξ_c Eq. (25) can be expanded to give four simultaneous equations for the $t^{(p)}$ given by

$$N-1+(-1)^q\exp(-im\omega_r T)\left\{2\sum_{p=1}^{q}(-1)^p\exp\left(im\omega_r t^{(p)}\right)+1\right\}=0 \quad (26)$$

for $m=\pm1$ and $m=\pm2$.

3. Timings

3.1. Analytical solutions for four-pulse sequences

For a sequence consisting of four π-pulses with a total duration equal to an integer number of rotor periods $n\tau_r$ Eq. (26) for the timings simplifies to

$$N-1+\left\{2\sum_{p=1}^{4}(-1)^p\exp\left(im\omega_r t^{(p)}\right)+1\right\}=0 \quad (27)$$

for both $m=\pm1$ and $m=\pm2$. Analytical solutions for four pulses can be found by following the procedure used by Antzutkin et al. [21] for finding TOSS timings. The four equations which make up the real and imaginary parts of Eq. (27) can be transformed to a new system

$$\begin{aligned}&\sin(\alpha/2)\cos(\beta/2)-\sin(\gamma/2)\cos(\delta/2)=0,\\&\sin\alpha\cos\beta-\sin\gamma\cos\delta=0,\\&-\cos(\alpha/2)\cos(\beta/2)+\cos(\gamma/2)\cos(\delta/2)+N/4=0,\\&-\cos\alpha\cos\beta+\cos\gamma\cos\delta+N/4=0,\end{aligned} \quad (28)$$

where $\alpha=\omega_r(t^{(1)}+t^{(3)})$, $\beta=\omega_r(t^{(3)}-t^{(1)})$, $\gamma=\omega_r(t^{(2)}+t^{(4)})$, and $\delta=\omega_r(t^{(4)}-t^{(2)})$. The first pair of Eq. (28) are satisfied trivially for $\sin(\alpha/2)=\sin(\gamma/2)=0$, such that $\alpha=2\pi k_1$ and $\gamma=2\pi k_2$ where k_1 and k_2 are integers. Under these circumstances the second pair becomes

$$\begin{aligned}&-(-1)^{k_1}\cos(\beta/2)+(-1)^{k_2}\cos(\delta/2)+N/4=0\\&\{\cos(\beta/2)+\cos(\delta/2)\}\{\cos(\beta/2)-\cos(\delta/2)\}+N/8=0\end{aligned} \quad (29)$$

and their solutions are

$$\begin{aligned}\beta&=2(-1)^{k_3}\cos^{-1}\left\{\frac{(-1)^{k_1}}{8}(N+2)\right\}+4\pi k_5,\\\delta&=2(-1)^{k_4}\cos^{-1}\left\{\frac{(-1)^{k_2+1}}{8}(N-2)\right\}+4\pi k_6,\end{aligned} \quad (30)$$

where k_1–k_6 are integers. Hence, possible timings are given by

$$\begin{aligned}\omega_r t^{(1)}&=\pi(k_1-2k_5)-(-1)^{k_3}\cos^{-1}\left\{\frac{(-1)^{k_1}}{8}(N+2)\right\},\\\omega_r t^{(2)}&=\pi(k_2-2k_6)-(-1)^{k_4}\cos^{-1}\left\{\frac{(-1)^{k_2+1}}{8}(N-2)\right\},\\\omega_r t^{(3)}&=\pi(k_1+2k_5)+(-1)^{k_3}\cos^{-1}\left\{\frac{(-1)^{k_1}}{8}(N+2)\right\},\\\omega_r t^{(4)}&=\pi(k_2+2k_6)+(-1)^{k_4}\cos^{-1}\left\{\frac{(-1)^{k_2+1}}{8}(N-2)\right\}.\end{aligned} \quad (31)$$

Real solutions to Eq. (28) lie in the range $-6<N<6$, and therefore the maximum amplification factor which can be achieved using four π-pulses is $N=6$. Realizable four-pulse sequences with an accessible spin echo must have all $t^{(p)}>0$ and $t^{(1)}<t^{(2)}<t^{(3)}<t^{(4)}<T$. Examples of short realizable four-pulse sequences for amplification factors $2<N<6$ are given in Table 1 with timings as fractions of a rotor period. Note that all these sequences last two rotor periods, and that an amplification factor of 6 can be achieved with three π-pulses and a phase reversal of φ_1 and φ_4. Longer sequences with different values for k_i can be used at high MAS rates to avoid overlap of pulses. Numerical searches for timings have not produced any additional values.

3.2. Analytical solutions for five-pulse sequences

An attempt to find general sequences which contain more than four π-pulses results in an under-determined Eq. (26). However, sequences which contain five π-pulses symmetrically disposed about $T/2$ with a total duration equal to an integer number of rotor periods can be found and were discussed in [19]. In this case $T=n\tau_r$, $t^{(3)}=T/2$, $t^{(4)}=T-t^{(2)}$, $t^{(5)}=T-t^{(1)}$, the imaginary part of Eq. (26) is zero and the equation system becomes

$$\begin{aligned}&4\cos\left(\omega_r t^{(1)}\right)-4\cos\left(\omega_r t^{(2)}\right)+N+2(-1)^n-2=0,\\&4\cos\left(2\omega_r t^{(1)}\right)-4\cos\left(2\omega_r t^{(2)}\right)+N=0.\end{aligned} \quad (32)$$

Table 1
Examples of the shortest realizable pulse timings $t^{(p)}$ for four-pulse sequences

$N(k_1,k_2)$[a]	$t^{(1)}/\tau_r$	$t^{(2)}/\tau_r$	$t^{(3)}/\tau_r$	$t^{(4)}/\tau_r$	T/τ_r
2(1,2)	0.16667	0.75000	0.83333	1.25000	2.00000
3(1,2)	0.14255	0.73005	0.85735	1.26995	2.00000
4(1,2)	0.11503	0.70978	0.88497	1.29022	2.00000
5(1,2)	0.08043	0.68882	0.91957	1.31118	2.00000
6(1,2)	0.00000	0.66667	1.00000	1.33333	2.00000

[a] All other k_i are 0 for the these solutions.

Solutions for timings in sequences with n even and odd are given by

$$\omega_r t^{(1)} = \pi - (-1)^{k_1} \cos^{-1}\left(\frac{N-2}{8}\right) + 2\pi k_3,$$
$$\omega_r t^{(2)} = (-1)^{k_2} \cos^{-1}\left(\frac{N+2}{8}\right) + 2\pi k_4 \quad (33)$$

and

$$\omega_r t^{(1)} = \pi - (-1)^{k_1} \cos^{-1}\left(\frac{16+N^2-10N}{8(N-4)}\right) + 2\pi k_3,$$
$$\omega_r t^{(2)} = (-1)^{k_2} \cos^{-1}\left(\frac{16+N^2-6N}{8(N-4)}\right) + 2\pi k_4, \quad (34)$$

respectively, where k_1–k_4 are integers. For n odd there are real solutions to Eq. (32) in the ranges $-3.12 < N < 3.12$ and $6 < N < 8$, while for n even there are solutions in the range $-6 < N < 6$, so that the maximum amplification factor which can be achieved using five π-pulses is $N = 8$. Examples of short five-pulse sequences for amplification factor $2 < N < 8$ were given previously in Table 2 of [19].

3.3. Analytical solutions for seven-pulse sequences

The form of Eq. (26) suggests that symmetrical sequences of duration $T = 4\tau_r$ with $t^{(2)} = T/4$, $t^{(4)} = T/2$, $t^{(5)} = T - t^{(3)}$, $t^{(6)} = T - t^{(2)}$, and $t^{(7)} = T - t^{(1)}$ should give large amplification factors. For these sequences the equation system becomes

$$4\cos\left(\omega_r t^{(1)}\right) + 4\cos\left(\omega_r t^{(3)}\right) + N - 8 = 0,$$
$$4\cos\left(2\omega_r t^{(1)}\right) + 4\cos\left(2\omega_r t^{(3)}\right) + N - 8 = 0 \quad (35)$$

and solutions are given by

$$\omega_r t^{(1)} = (-1)^{k_1} \cos^{-1}\left(1 - \frac{N}{8} + \frac{\sqrt{12N-N^2}}{8}\right) + 2\pi k_3,$$
$$\omega_r t^{(3)} = (-1)^{k_2} \cos^{-1}\left(1 - \frac{N}{8} - \frac{\sqrt{12N-N^2}}{8}\right) + 2\pi k_4, \quad (36)$$

where k_1–k_4 are integers. There are real solutions in the range $6 < N < 12$ and examples of realizable seven-pulse sequences with well-spaced pulses and $N > 8$ are shown in Table 2.

4. Experimental

The pulse sequence used here to record two-dimensional MAS spectra with CSA amplification in the ω_1 dimension is shown in Fig. 2. The t_1 time is incremented by some convenient fraction, usually 1/16 or 1/32, of the rotor period and the timings of the π-pulses are given above. In order to reconstruct the required two-dimensional FID two experiments are necessary in which the phase of the carbon-13 $\pi/2$ storage pulse φ_3 is alternated $\pi/2, \pi$ or $3\pi/2, 0$ when using sequences with an odd or even number of pulses, respectively. The two experiments can be combined in the receiver by simultaneously shifting the reference phase from 0 to $\pi/2$. Further phase cycling of the carbon-13 pulses selects changes in coherence order $\Delta p = \pm 1$ with φ_1 and φ_4 and $\Delta p = 0, \pm 2$ across the whole of each sequence with φ_2 and φ_5. A possible phase cycle and sample pulse programs are available on the Website http://www.nott.ac.uk/~pczjt/.

In common with 2D-PASS there is no need to retain pure absorption two-dimensional lineshapes, because the periodic nature of the signal in the indirect dimension ensures that there is no linewidth in ω_1. Reconstruction of the required FID in the receiver as described above allows the two-dimensional spectrum to be obtained by straightforward complex Fourier transformation with respect to both t_1 and t_2, after weighting as normal in the detection dimension. However, in order to preserve the periodic signal in t_1, it is important that no weighting functions are applied in the indirect dimension prior to Fourier transformation. Although the two-dimensional peaks which result are of mixed phase, the vanishing ω_1 linewidth means that there is no detrimental effect on the spectrum. Phase corrections in ω_2 are made by inspecting the $\omega_1 = 0$ slice of the two-dimensional spectrum. An additional first order correction in ω_1 is usually required because of the finite widths of the $\pi/2$ storage pulses. Finite pulse length effects and other errors are discussed in more detail below. It should be noted that, because of the reversal of the sign of t_1 in Eq. (22), sidebands at $\omega_1 = j\omega_r$ with j negative appear at positive frequencies in ω_1 and vice versa.

This somewhat non-standard processing procedure is illustrated in Fig. 3 which shows a carbon-13 CSA amplification experiment for DL-tryptophan recorded at a Larmor frequency of 75.47 MHz and a MAS rate of

Table 2
Examples of the shortest realizable pulse timings $t^{(p)}$ for seven-pulse sequences

$N(k_3,k_4)$[a]	$t^{(1)}/\tau_r$	$t^{(2)}/\tau_r$	$t^{(3)}/\tau_r$	$t^{(4)}/\tau_r$	$t^{(5)}/\tau_r$	$t^{(6)}/\tau_r$	$t^{(7)}/\tau_r$	T/τ_r
9(0,1)	0.16212	1.00000	1.39100	2.00000	2.60900	3.00000	3.83788	4.00000
10(0,1)	0.20000	1.00000	1.40000	2.00000	2.60000	3.00000	3.80000	4.00000
11(0,1)	0.24370	1.00000	1.39485	2.00000	2.60515	3.00000	3.75630	4.00000
12(0,1)	0.33333	1.00000	1.33333	2.00000	2.66667	3.00000	3.66666	4.00000

[a] All other k_i are 0 for these solutions.

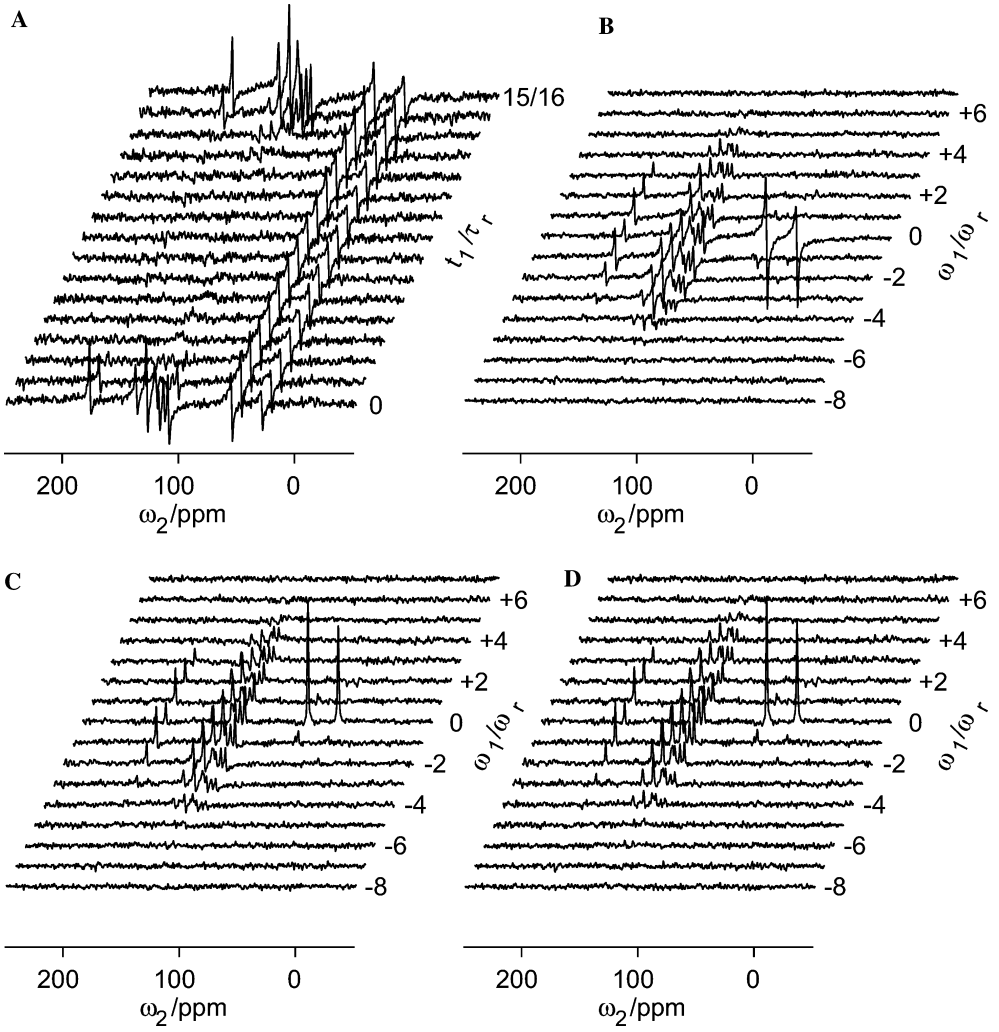

Fig. 3. Processing procedure for the CSA amplification experiment. (A) Interferograms produced after weighting in t_2, followed by complex Fourier transformation with respect to t_2. (B) Spectrum resulting from a subsequent Fourier transformation with respect to t_1. (C) Spectrum after phase correction in ω_2 in which the $\omega_1 = 0$ slice is purely absorptive, while a small ω_1-dependent phase error is apparent across the rest of the spectrum. (D) Spectrum after application of a frequency-dependent phase correction in ω_1. This carbon-13 CSA amplification experiment for DL-tryptophan was recorded at a Larmor frequency of 75.47 MHz, spinning at 10 kHz in a 4 mm MAS probe. A sequence with five π-pulses and an amplification factor of 8 was chosen, resulting in an apparent rate of 1.25 kHz in the ω_1 dimension. The MAS rate was stabilized to ±10 Hz. The contact time was 1.5 ms, the proton decoupling field strength was 100 kHz, and the acquisition period lasted 41 ms. The full spectral width was 50 kHz, and there were 16 t_1 values in total with an increment of 6.25 μs. The carbon-13 π-pulse length was 5.5 μs.

10 kHz. An amplification factor of 8 was chosen, resulting in an apparent rate of 1.25 kHz in the ω_1 dimension. Further experimental details are given in the figure caption. The interferograms produced after weighting in t_2, followed by complex Fourier transformation with respect to t_2 are shown in (A), while the spectrum resulting from a complex Fourier transformation with respect to t_1 is shown in (B). The effect of phase correction in ω_2 is shown in (C) in which the $\omega_1 = 0$ slice is purely absorptive, while a small ω_1-dependent phase error is apparent across the rest of the spectrum. Finally, (D) shows the result of applying a frequency-dependent phase correction in ω_1. Note that because of the mixed phase nature of the lineshapes, any phase correction in ω_1 affects the appearance of the spectrum in the ω_2 dimension. Fig. 3 also illustrates that with relatively broad shift anisotropies when spinning at faster MAS rates CSA amplification serves as an alternative to 2D-PASS, producing similar spectra with comparable sensitivity.

The following precautions serve to improve the quality of the CSA amplification spectra. Heteronuclear decoupling is interrupted during carbon-13 π-pulses to avoid unwanted Hartmann–Hahn contacts, and the delays between the π-pulses are reduced in order to take account of their finite length. The experiment requires careful calibration of the π-pulses to reduce sideband phase and amplitude distortions, and the quality of the sideband suppression in a TOSS sequence with the same number of π-pulses is a suitable calibration criterion.

The effects of experimental imperfections, and to a lesser extent resonance offsets, can be reduced in the case of the five-pulse sequences by shifting the relative phases of successive π-pulses through the series 0°, 330°, 60°, 330°, and 0°, a procedure which has been used in a similar context by Antzutkin et al. [21]. For four- and seven-pulse sequences a similar level of compensation can be achieved by replacing the π-pulses by composite pulses, such as $(\pi/2)_0\pi_{\pi/2}(\pi/2)_0$ [22]. Unless otherwise stated, all experimental CSA amplification spectra shown in this paper were recorded using the first of these methods.

5. Results and discussion

5.1. Demonstration

Fig. 4 illustrates that the sideband intensities obtained in the ω_1 dimension using CSA amplification are identical to those observed in the normal MAS spectrum at the apparent rate. A typical carbon-13 CSA amplification spectrum of glycine[1-^{13}C] recorded at a Larmor frequency of 75.47 MHz with a MAS rate of 12.5 kHz is shown in (A). At this MAS rate spinning sidebands in the ω_2 dimension are negligible. In this particular case an amplification factor of 10 was chosen, resulting in an apparent rate of 1.25 kHz in the ω_1 dimension and composite π-pulses were used. Further details are given in the figure caption. A series of spectra were recorded at different MAS rates with amplification factors chosen so that the apparent rate remained 1.25 kHz. The ω_1 sideband intensities measured for the glycine carbonyl site from the whole series are compared in (B) (symbols) which also shows those obtained from the normal MAS spectrum at 1.25 kHz (line). The good agreement between the sideband intensities demonstrates that CSA amplification functions correctly.

As a further test of CSA amplification, the principal components of the shift tensors of methyl-α-D-glucopyranoside were extracted from the ω_1 sideband intensities measured from the spectrum of Fig. 1(B). The results, obtained using a fitting procedure based on the method of Herzfeld and Berger [3], are shown in Table 3. Since Eq. (17) involves a projection onto the ω_1 axis, the contributions from any residual sidebands in the ω_2 dimension were included in the total for each ω_1 intensity. This procedure is necessary to obtain accurate values of the principal components. Problems arising from overlap of ω_2 sidebands from different chemical sites are minimized by the relatively high MAS rates which can be used with CSA amplification. For comparison the average of three separate measurements from the literature [6,23,24] are also shown in Table 3.

The difference between the principal components derived from the CSA amplification and the average of the literature values rarely exceeds 2 ppm, while the spread of the literature values is as much as 5 ppm for some sites. Of particular note is site (1), for which values of the asymmetry (defined as $\eta = (\sigma_{22} - \sigma_{11})/(\sigma_{33} - \sigma_{iso})$ with $|\sigma_{33} - \sigma_{iso}| > |\sigma_{11} - \sigma_{iso}| > |\sigma_{22} - \sigma_{iso}|$) between 0 and 0.44 have been reported previously. The CSA amplification measurement for this site results in principal components which agree to within 2 ppm with those

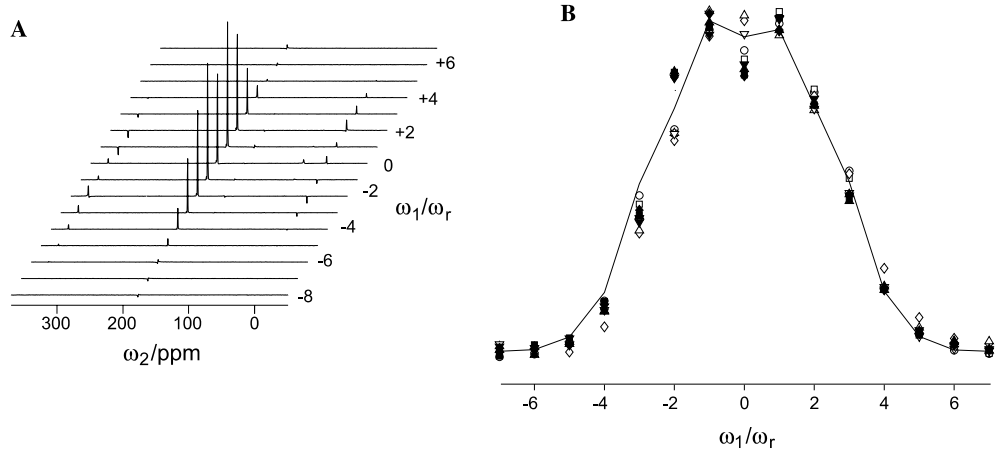

Fig. 4. (A) Carbon-13 CSA amplification spectrum of glycine[1-^{13}C] recorded at a Larmor frequency of 75.47 MHz, spinning at 12.5 kHz in a 4 mm MAS probe. A sequence with seven π-pulses and an amplification factor of 10 was chosen, resulting in an apparent rate of 1.25 kHz in the ω_1 dimension. Composite π-pulses of the type $(\pi/2)_0\pi_{\pi/2}(\pi/2)_0$ were used. The MAS rate was stabilized to ±10 Hz. The contact time was 1.5 ms, the proton decoupling field strength was 100 kHz, and the acquisition period lasted 41 ms. The full spectral width was 50 kHz, and there were 16 t_1 values in total with an increment of 5.0 μs. The carbon-13 π-pulse length was 5.0 μs. (B) Sideband intensities from a series of similar spectra recorded at different MAS rates with amplification factors chosen so that the apparent rate remained 1.25 kHz. Reduction factors were: open circle 4, open square 5, open diamond 6, open upward triangle 7, open downward triangle 8, filled diamond 9, filled upward triangle 10, filled downward triangle 11, filled square: 12. Sideband intensities obtained from the normal MAS spectrum at 1.25 kHz are shown with a solid line.

Table 3
CSA amplification measurements of principal components of shift tensors in methyl-α-glucopyranoside and comparison with literature values

Site[a]	σ_{11} (ppm)[b]	σ_{22} (ppm)	σ_{33} (ppm)
1	92 (89)[c]	95 (93)	118 (119)
4	61 (57)	73 (73)	94 (95)
3	59 (58)	72 (70)	95 (95)
2,5	89 (87)	77 (77)	54 (52)
6	90 (89)	67 (69)	36 (33)
7	89 (87)	70 (72)	12 (12)

[a] Sites are labelled in accordance with Sastry et al. [23].
[b] Principal components are labelled according to the convention $|\sigma_{22} - \sigma_{iso}| < |\sigma_{11} - \sigma_{iso}| < |\sigma_{33} - \sigma_{iso}|$.
[c] Numbers in brackets are the average of the literature values [6,23,24].

obtained in a single crystal study by Sastry et al. [23]. The good agreement shown in Table 3 demonstrates that the principal components can be obtained accurately using CSA amplification. The fact that the spectrum in Fig. 1(B) was recorded with just 48 scans per t_1 increment indicates the reasonable sensitivity of the method.

5.2. Reliability of sideband patterns

The theory of CSA amplification described above assumes π-pulses which are infinitesimally short, exactly synchronized with the MAS rotor and correctly calibrated. In practice, experimental imperfections, such as finite RF amplitude, fluctuations in the MAS rate and B_1 inhomogeneity, as well as off-resonance effects are expected to cause ω_1 sideband intensities to deviate from the values expected for ω_r/N. The experimental results described above demonstrate that such deviations are sufficiently small to allow accurate values of the principal components to be measured using CSA amplification. However, in order to investigate the role of experimental imperfections and off-resonance effects further, simulations have been carried out using the SIMPSON program due to Bak et al. [25].

The simulations shown here involve a carbon-13 nucleus with a chemical shift anisotropy (defined as $\delta = \sigma_{33} - \sigma_{iso}$) of 25 ppm and an asymmetry of 0.25. In each case the Larmor frequency was 75.47 MHz and the MAS rate was 3.2 kHz. CSA amplification by a factor 8 was achieved using a 5-pulse sequence, giving an apparent rate of 400 Hz in the ω_1 dimension. The two-dimensional FID which results from this sequence was generated with 16 t_1 increments and 256 acquisition points by direct calculation of the full MAS propagators for the entire pulse sequence, including the effect of finite RF amplitude. Powder averaging was achieved using 20 (α, β) orientations, following the REPULSION scheme [26] and 40 uniformly distributed γ values. Zero-filling to 1024 points and line broadening were applied in ω_2 before a double complex Fourier transform to produce the two-dimensional spectrum. Many simulations were carried out with other CSA tensors, MAS rates and amplification factors, but the overall assessment of the reliability of CSA amplification was unchanged.

Experimental imperfections distort the CSA amplification spectrum in two distinct ways. The first is the introduction of a ω_1-dependent phase error which, because of the phase-twist nature of the two-dimensional lineshapes, is apparent in ω_2. In order to illustrate this, the CSA amplification spectrum simulated using ideal pulses with infinite RF amplitude is shown in Fig. 5(A). Similar simulations are shown in (B) for a RF amplitude of 60 kHz and (C) with an actual MAS rate which deviates by 20 Hz from the nominal rate of 3.2 kHz used to calculate the pulse timings. A small, but appreciable, ω_1-dependent phase error arises in (B) because of the finite length of the $\pi/2$ storage pulses and in (C) because of the loss of rotor synchronization in t_1. However, it should be noted that these distortions can be eliminated by a phase correction, as shown in Fig. 3. Only finite RF

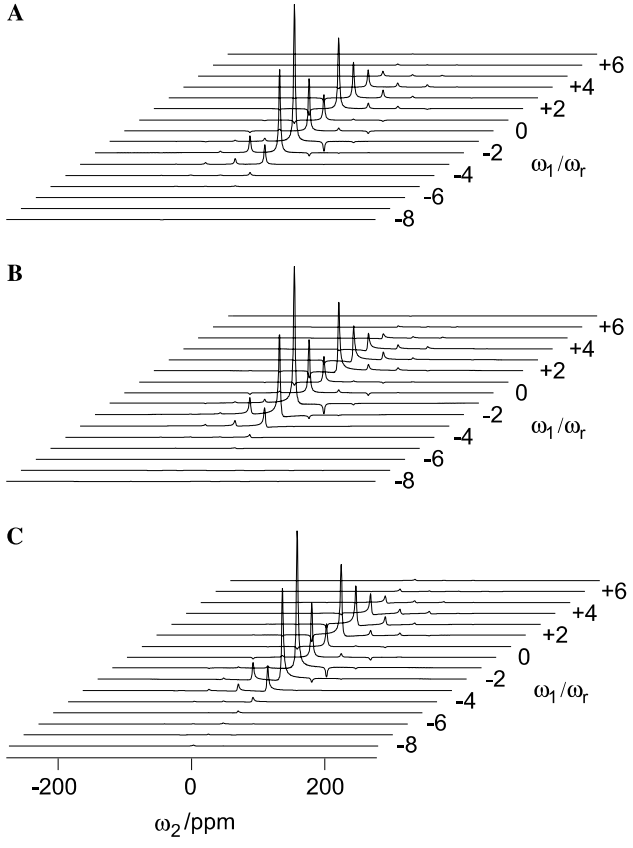

Fig. 5. Simulated CSA amplification spectra, produced as described in the text using (A) ideal pulses with infinite RF amplitude, (B) a RF amplitude of 60 kHz and (C) an actual MAS rate which deviates by 20 Hz from the nominal rate. Note that the delays between pulses in (B) were reduced to compensate for their length. The main effect of both finite rf amplitude and fluctuation in the MAS rate is a ω_1-dependent phase error.

amplitude makes an appreciable contribution under the experimental conditions used here, since the MAS rate can be stabilized to within ±1 Hz.

More critical is the effect that experimental imperfections have on the reliability of the sideband patterns produced. In order to investigate this aspect further, the mismatch between the sideband intensities simulated for CSA amplification and those expected from MAS is quantified using the parameter

$$\chi^2 = \sum_j \left(I_j - I_j^{\mathrm{MAS}}\right)^2. \tag{37}$$

In our experience for the parameters used here χ^2 must remain below 1.0 to give an acceptable error of less than 2 ppm in the principal components of shift tensors measured using CSA amplification.

Fig. 6 illustrates the effect of fluctuations in the MAS rate. Three sets of simulations were carried out in which the actual rate deviated from the nominal rate of 3.2 kHz by up to ±50 Hz and the RF amplitude was 60 kHz (solid line), 100 kHz (dashes) and 140 kHz (dots), respectively. The resulting plots of the mismatch parameter χ^2 against the actual rate indicate that CSA amplification is robust with respect to fluctuations in the MAS rate. Provided that the MAS rate can be stabilized to within ±10 Hz, the mismatch between the CSA amplification sideband pattern and that expected for MAS is insignificant. However, if the actual MAS rate deviates from the nominal rate by more than ±40 Hz, the errors in the measured shift tensor become unacceptable. The detailed shape of the plots varies substantially with the CSA tensor, nominal MAS rate and amplification factor, but the range of actual rates which give reliable results remains similar.

Fig. 7 illustrates the effect of pulse length miscalibration and B_1 inhomogeneity. Three sets of simulations were carried out in which the flip angle of the π-pulses deviated from 180° by up to ±50°. For the first set (solid line) the phase of successive π-pulses remained constant, while for the second set (dots) they were shifted through the series 0°, 330°, 60°, 330°, and 0° as described above. For the third set (dashes) the π-pulses were replaced by composite pulses of the form $(\pi/2)_0\pi_{\pi/2}(\pi/2)_0$. The RF amplitude was 60 kHz in all three cases. The resulting plots indicate that if the π-pulses in the CSA amplification experiment have constant phases, a miscalibration of ±10° is sufficient to result in an unacceptable error in the measured shift tensor. Given the B_1 inhomogeneity of commercial MAS probes, this degree of accuracy in calibration may not be achievable for the whole sample without restricting its volume. However, a substantial improvement is obtained by the simple expedient of shifting the phases of successive π-pulses as described above. In this case miscalibration up to ±20° gives an acceptable error in the measured CSA tensor. Substituting composite pulses for the π-pulses gives a further level of compensation, as confirmed experimentally in Fig. 4.

Fig. 8 illustrates the effect of resonance offset which is expected to be significant, since the experiment contains a number of π-pulses. Three sets of simulations were carried out in which the isotropic shift was varied between ±20 kHz and the RF amplitude was 60 kHz. These correspond to the simulated experiments

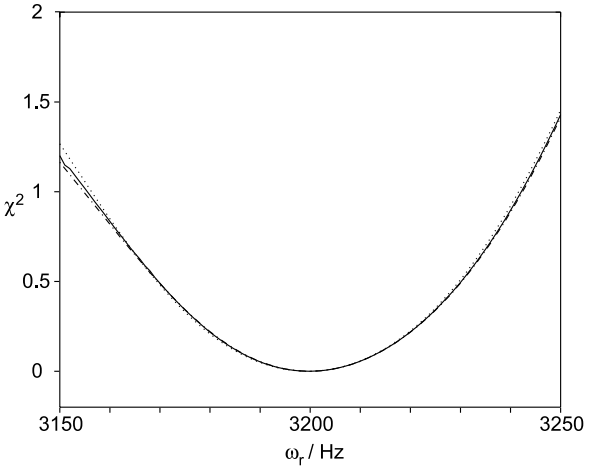

Fig. 6. Simulations which illustrate the effect on the reliability of the CSA amplification experiment of fluctuations in the MAS rate. The plot shows the mismatch parameter χ^2 described in the text as a function of the actual MAS rate for simulated CSA amplification experiments with a nominal MAS rate of 3200 Hz. The RF amplitude was 60 (solid line), 100 (dashes), and 140 (dots) kHz.

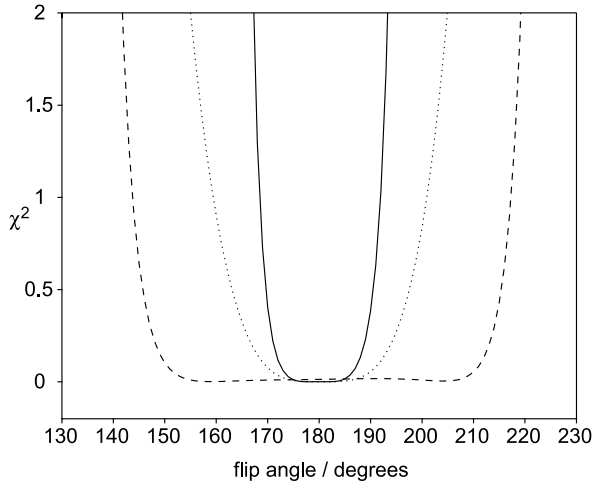

Fig. 7. Simulations which illustrate the effect on the reliability of the CSA amplification experiment of pulse length miscalibration or B_1 inhomogeneity. The plot shows the mismatch parameter χ^2 described in the text as a function of the actual flip angle of the π-pulses for simulated CSA amplification experiments using π-pulses with a constant phase (solid line), with phases shifted through the series 0°, 330°, 60°, 330°, 0° (dots) and replaced by $(\pi/2)_0\pi_{\pi/2}(\pi/2)_0$ composite pulses (dashes).

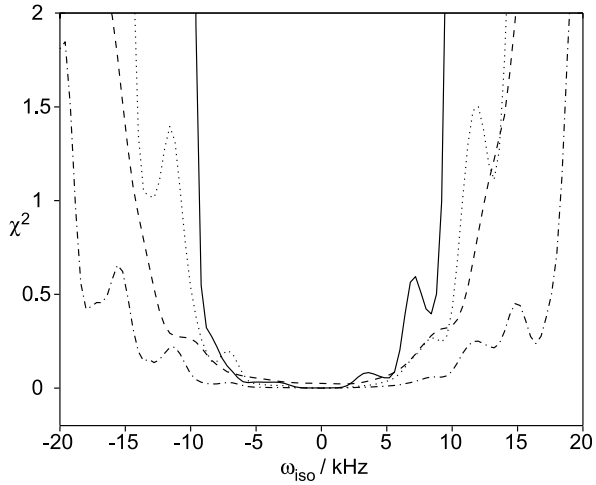

Fig. 8. Simulations which illustrate the effect on the reliability of the CSA amplification experiment of resonance offset. The plot shows the mismatch parameter χ^2 described in the text as a function of the isotropic shift for simulated CSA amplification experiments using a RF amplitude of 60 kHz and π-pulses with a constant phase (solid line), with phases shifted through the series 0°, 330°, 60°, 330°, 0° (dots) and replaced by $(\pi/2)_0\alpha_{\pi/2}(\pi/2)_0(\alpha = 240°)$ composite pulses (dashes). A further simulation with an increased RF amplitude of 100 kHz and π-pulses with phases shifted through the series 0°, 330°, 60°, 330°, 0° is also shown (dots and dashes).

described in Fig. 7, except that the composite pulses used for the third set were of the form $(\pi/2)_0\alpha_{\pi/2}(\pi/2)_0$ with $\alpha = 240°$ [27]. The fourth set (dots and dashes) is equivalent to the second, but with the RF amplitude increased to 100 kHz. A notable feature of all these plots is their asymmetry. The plot shows that, contrary to expectations, CSA amplification is reliable in the presence of quite significant resonance offsets.

5.3. Comparison with other methods

Several other experiments which correlate fast and slow spinning sideband patterns have been suggested. In contrast to the CSA amplification method described here, these are not based on 2D-PASS, but involve the insertion of π-pulses directly into the evolution period. In the spin-echo experiment of Kolbert et al. [28] $N - 1$ π-pulses divide t_1 into N equally spaced intervals and delay the formation of rotational echoes, leading to the observation of ω_1 sidebands at ω_r/N. This method was demonstrated experimentally for $N < 8$. However, for $N > 2$ the sideband patterns produced are not identical to those obtained with MAS. In addition, the experiment results in mixed-phase two-dimensional lineshapes. Nevertheless, the spin-echo method has the advantage of simplicity, and requires only a small number of π-pulses. XCS [29] is a related constant time experiment in which t_1 determines the position of $N/2$π-pulses within a fixed delay of duration $N\tau_r$ This method was demonstrated experimentally for $N = 6$. Isotropic shifts can be eliminated from t_1 using two complementary spectra and a special transformation. Hence, a minimal number of t_1 increments suffices to sample the periodic evolution under the anisotropic shift, so long as transverse relaxation can be neglected. In contrast to the spin-echo method, the sideband patterns produced are identical to those obtained with MAS. Very high values of N up to 30 have been observed using the recently proposed ROSES method [30]. In this experiment, the chemical shift evolution is interrupted for a part of each t_1 increment by a pair of refocusing π-pulses. Once again, the sideband patterns are different from those observed with MAS. In addition, a scaled isotropic shift remains in t_1, so that many increments are necessary. For long t_1 times the number of π-pulses is very large, and the experiment is expected to be sensitive to off-resonance effects. To date, none of these three methods has been assessed for their reliability.

The main advantage of the CSA amplification experiment is that of the 2D-PASS experiment on which it is based. The genuine periodicity of the t_1 evolution under the anisotropic shift means that long two-dimensional experiments can be avoided. In addition, only a small number of π-pulses are required, even for the largest amplification factors. Transverse relaxation during the sequences of q π-pulses causes loss of signal, but the coincidence of rotor and spin echoes at the end limits this to the contribution from the homogeneous T_2. Finally, the sideband patterns produced are identical to those obtained with MAS at a rate ω_r/N. At this stage, the main drawback appears to be that the addition of extra π-pulses to symmetrical sequences once $q > 7$ results in a diminishing gain in the maximum amplification factor.

6. Conclusions

An CSA amplification experiment which correlates a fast MAS spectrum with the sideband pattern expected for ω_r/N has been described in detail. New sequences with seven π-pulses allow amplification factors as high as 12. Measurements of narrow shift anisotropies can be made with moderate MAS rates. These have been shown to be reliable under normal experimental conditions. In addition, the experiment functions as an alternative to 2D-PASS at fast MAS rates.

Acknowledgments

This research was supported by the EPSRC (Grants GR/L26742 and GR/N02023, as well as a studentship for C.C.). H.G. thanks the Royal Society for a University Research Fellowship, and L.S. is a recipient of an ORS Scholarship.

References

[1] W.S. Veeman, Prog. Nucl. Magn. Reson. Spectrosc. 16 (1984) 193.
[2] M.M. Maricq, J.S. Waugh, J. Chem. Phys. 70 (1979) 3300.
[3] J. Herzfeld, A.E. Berger, J. Chem. Phys. 73 (1980) 6021.
[4] Y. Yarim-Agaev, P.M. Tutunjian, J.S. Waugh, J. Magn. Reson. 47 (1982) 51.
[5] A. Bax, N.M. Szeverenyi, G.E. Maciel, J. Magn. Reson. 51 (1983) 400.
[6] R. Tycko, G. Dabbagh, P. Mirau, J. Magn. Reson. 85 (1989) 265.
[7] Z. Gan, D.M. Grant, R.R. Ernst, Chem. Phys. Lett. 254 (1996) 349.
[8] J.D. Gross, P.R. Costa, R.G. Griffin, J. Chem. Phys. 108 (1998) 7286.
[9] Bax, N.M. Szeverenyi, G.E. Maciel, J. Magn. Reson. 55 (1983) 494.
[10] T. Terao, T. Fujii, T. Onodera, A. Saika, Chem. Phys. Lett. 107 (1984) 145.
[11] L. Frydman, G.C. Chingas, Y.K. Lee, P.J. Grandinetti, M.A. Eastman, G.A. Barrall, A. Pines, J. Chem. Phys. 97 (1992) 4800.
[12] A.C. Kolbert, R.G. Griffin, Chem. Phys. Lett. 100 (1990) 130.
[13] W.T. Dixon, J. Chem. Phys. 77 (1982) 1800.
[14] Z. Gan, J. Am. Chem. Soc. 114 (1992) 8307.
[15] J.Z. Hu, D.W. Alderman, C. Ye, R.J. Pugmire, D.M. Grant, J. Magn. Reson. A 105 (1993) 82.
[16] W.T. Dixon, J. Magn. Reson. 44 (1981) 220.
[17] S. Féaux de Lacroix, J.J. Titman, A. Hagemeyer, H.W. Spiess, J. Magn. Reson. 97 (1992) 435.
[18] O.N. Antzutkin, S.C. Shekar, M.H. Levitt, J. Magn. Reson. A 115 (1995) 7.
[19] C. Crockford, H. Geen, J.J. Titman, Chem. Phys. Lett. 344 (2001) 367.
[20] C. Crockford, H. Geen, J.J. Titman, Solid-State NMR 22 (2002) 298.
[21] O.N. Antzutkin, Z. Song, X. Feng, M.H. Levitt, J. Chem. Phys. 100 (1994) 130.
[22] M.H. Levitt, R. Freeman, J. Magn. Reson. 33 (1979) 473.
[23] D.L. Sastry, K. Takegoshi, C.A. McDowell, Carbohydr. Res. 165 (1987) 161.
[24] R.C. Ziegler, R.A. Wind, G.E. Maciel, J. Magn. Reson. 79 (1988) 299.
[25] M. Bak, J.T. Rasmussen, N.C. Nielsen, J. Magn. Reson. 147 (2000) 296.
[26] M. Bak, N.C. Nielsen, J. Magn. Reson. 125 (1997) 132.
[27] R. Freeman, S.P. Kempsell, M.H. Levitt, J. Magn. Reson. 38 (1980) 453.
[28] A.C. Kolbert, D.P. Raleigh, M.H. Levitt, R.G. Griffin, J. Chem. Phys. 90 (1989) 679.
[29] T. Gullion, J. Magn. Reson. 85 (1989) 614.
[30] B. Elena, S. Hediger, L. Emsley, J. Magn. Reson. 160 (2003) 40.